The FASEB Journal • Research Communication

Kv1.3 channel-blocking immunomodulatory peptides from parasitic worms: implications for autoimmune diseases

Sandeep Chhabra,*,[1] Shih Chieh Chang,*,[1] Hai M. Nguyen,[†,‡,1] Redwan Huq,[§,‖]
Mark R. Tanner,[§,¶] Luz M. Londono,[††] Rosendo Estrada,[‡‡] Vikas Dhawan,[‡‡]
Satendra Chauhan,[‡‡] Sanjeev K. Upadhyay,[†] Mariel Gindin,[§§,‖] Peter J. Hotez,[#,**]
Jesus G. Valenzuela,[‖] Biswaranjan Mohanty,* James D. Swarbrick,* Heike Wulff,[‡]
Shawn P. Iadonato,[††] George A. Gutman,[†] Christine Beeton,[§] Michael W. Pennington,[‡‡]
Raymond S. Norton,*,[2] and K. George Chandy[†,2]

*Medicinal Chemistry, Monash Institute of Pharmaceutical Sciences, Monash University, Parkville,
Victoria, Australia; [†]Department of Physiology and Biophysics, School of Medicine, University of
California, Irvine, California, USA; [‡]Department of Pharmacology, University of California, Davis,
California, USA; [§]Department of Molecular Physiology and Biophysics, [‖]Graduate Program in
Molecular Physiology and Biophysics, and [¶]Interdepartmental Graduate Program in Translational
Biology and Molecular Medicine, and [#]Sabin Vaccine Institute and **Texas Children's Hospital
Center for Vaccine Development, National School of Tropical Medicine, Baylor College of Medicine,
Houston, Texas, USA; [††]Kineta, Inc., Seattle, Washington, USA; [‡‡]Peptides International, Louisville,
Kentucky, USA; [§§]Department of Microbiology, Immunology, and Tropical Medicine, The George
Washington University, Washington D.C., USA; and [‖]Vector Molecular Biology Section, Laboratory
of Malaria and Vector Research, National Institutes of Allergy and Infectious Diseases, National
Institutes of Health, Bethesda, Maryland, USA

ABSTRACT   The voltage-gated potassium (Kv) 1.3
channel is widely regarded as a therapeutic target for
immunomodulation in autoimmune diseases. ShK-186,
a selective inhibitor of Kv1.3 channels, ameliorates
autoimmune diseases in rodent models, and human
phase 1 trials of this agent in healthy volunteers have
been completed. In this study, we identified and characterized a large family of *Stichodactyla helianthus* toxin
(ShK)–related peptides in parasitic worms. Based on
phylogenetic analysis, 2 worm peptides were selected
for study: AcK1, a 51-residue peptide expressed in the
anterior secretory glands of the dog-infecting hookworm *Ancylostoma caninum* and the human-infecting
hookworm *Ancylostoma ceylanicum*, and BmK1, the C-terminal domain of a metalloprotease from the filarial
worm *Brugia malayi*. These peptides in solution adopt
helical structures closely resembling that of ShK. At
doses in the nanomolar–micromolar range, they block
native Kv1.3 in human T cells and cloned Kv1.3 stably
expressed in L929 mouse fibroblasts. They preferentially suppress the proliferation of rat CCR7− effector
memory T cells without affecting naive and central
memory subsets and inhibit the delayed-type hypersensitivity (DTH) response caused by skin-homing effector
memory T cells in rats. Further, they suppress IFNγ
production by human T lymphocytes. ShK-related peptides in parasitic worms may contribute to the potential
beneficial effects of probiotic parasitic worm therapy in
human autoimmune diseases.—Chhabra, S., Chang,
S. C., Nguyen, H. M., Huq, R., Tanner, M. R., Londono, L. M., Estrada, R., Dhawan, V., Chauhan, S.,
Upadhyay, S. K., Gindin, M., Hotez, P. J., Valenzuela,
J. G., Mohanty, B., Swarbrick, J. D., Wulff, H., Iadonato, S. P., Gutman, G. A., Beeton, C., Pennington,
M. W., Norton, R. S., Chandy, K. G. Kv1.3 channel-blocking immunomodulatory peptides from parasitic
worms: implications for autoimmune diseases. *FASEB J.*
28, 000–000 (2014). www.fasebj.org

THE VOLTAGE-GATED POTASSIUM (Kv) 1.3 channel regulates the membrane potential of T cells and provides the counterbalancing K^+ efflux that promotes and sustains Ca^{2+} signaling during the activation response (1). Its important role in effector memory T (T_{EM}) cells ($CD4^+$ or $CD8^+$ T cells that are $CCR7^- CD45RA^-$) has made Kv1.3 an attractive therapeutic target for immunomodulation (1–6). In patients with multiple sclerosis (MS), type-1 diabetes mellitus, rheumatoid arthritis (RA), psoriasis, or chronic asthma, disease-associated T cells are Kv1.3-dependent T_{EM} cells, and selective Kv1.3 inhibitors suppress the proliferation and cytokine production of these cells; other T-cell subsets are not affected because they use the calcium-activated channel KCa3.1 to regulate membrane potential and calcium signaling (1, 3, 4, 6, 7). Kv1.3 blockers are effective in rodent models of delayed-type hypersensitivity (DTH), MS (experimental autoimmune encephalomyelitis), RA (pristane-induced arthritis), type-1 diabetes mellitus, contact dermatitis, allograft skin transplant, diet-induced obesity, chronic asthma, and inflammatory bone resorption in experimental periodontal disease (1–3, 8–15).

Several Kv1.3 inhibitors are under development as therapeutics. The most advanced is ShK-186, a synthetic analogue of the Kv1.3-blocking peptide, ShK, present in the sea anemone *Stichodactyla helianthus* (4). ShK and ShK-186 block Kv1.3 at picomolar concentrations by binding to and occluding the pore–vestibule region of Kv1.3 (1, 4, 16–19). ShK-186 is the subject of an open Investigational New Drug (IND) application in the United States and human phase 1A and 1B trials of this agent were recently completed in healthy volunteers.

The Simple Modular Architecture Research Tool (SMART) (available at http://smart.embl-heidelberg.de/) predicts the existence of a large superfamily of 668 proteins that contain 1315 domains resembling ShK (referred to as ShKT domains and peptides). ShKTs exist in both the plant and animal kingdoms, suggesting an ancient origin (20). The structures of 6 ShKTs have been determined, all of which have been reported to modulate ion channels (see the SMART database). The largest family of ShKTs is found in worms, with 276 of 668 proteins in the SMART database coming from worms (*Caenorhabditis elegans*, *C. briggsae*, *Brugia malayi*, *B. pahangi*, *Ancylostoma ceylanicum*, *Schistosoma mansoni*, and *Toxocara canis*).

Throughout their 200,000-year history, humans have carried parasitic worms in their bodies, some harmless and others causing disease (21, 22). Indeed, worm infections are among the most common afflictions of people living in poverty in the developing world, where they contribute to the healthcare burden of malnutrition, anemia, allergies, seizures, colitis, and growth retardation. Currently, approximately 876 million children annually require regular deworming to protect them from these debilitating diseases (23). In the developed world, worm infestations have greatly decreased, and it has been suggested that this reduction has contributed to the increased incidence of autoimmune diseases (21, 24, 25). In 2005, probiotic therapy with the nematode *Trichuris suis* was reported to have improved symptoms in patients with inflammatory bowel disease (24, 25). Subsequent studies confirmed the beneficial effects of probiotic worm therapy in humans and animal models of inflammatory bowel disease and MS, and human trials with probiotic worm therapy are now under way (21–52). The worm-dependent protective effect in autoimmune diseases is associated with increases in regulatory T cells, direct suppression of proinflammatory cytokines, and the induction of T_H2-type immune responses that indirectly counteract proinflammatory responses (27, 28, 36, 37, 39, 41, 48). It has also been suggested that worm infections alter the host microbiome (53, 54).
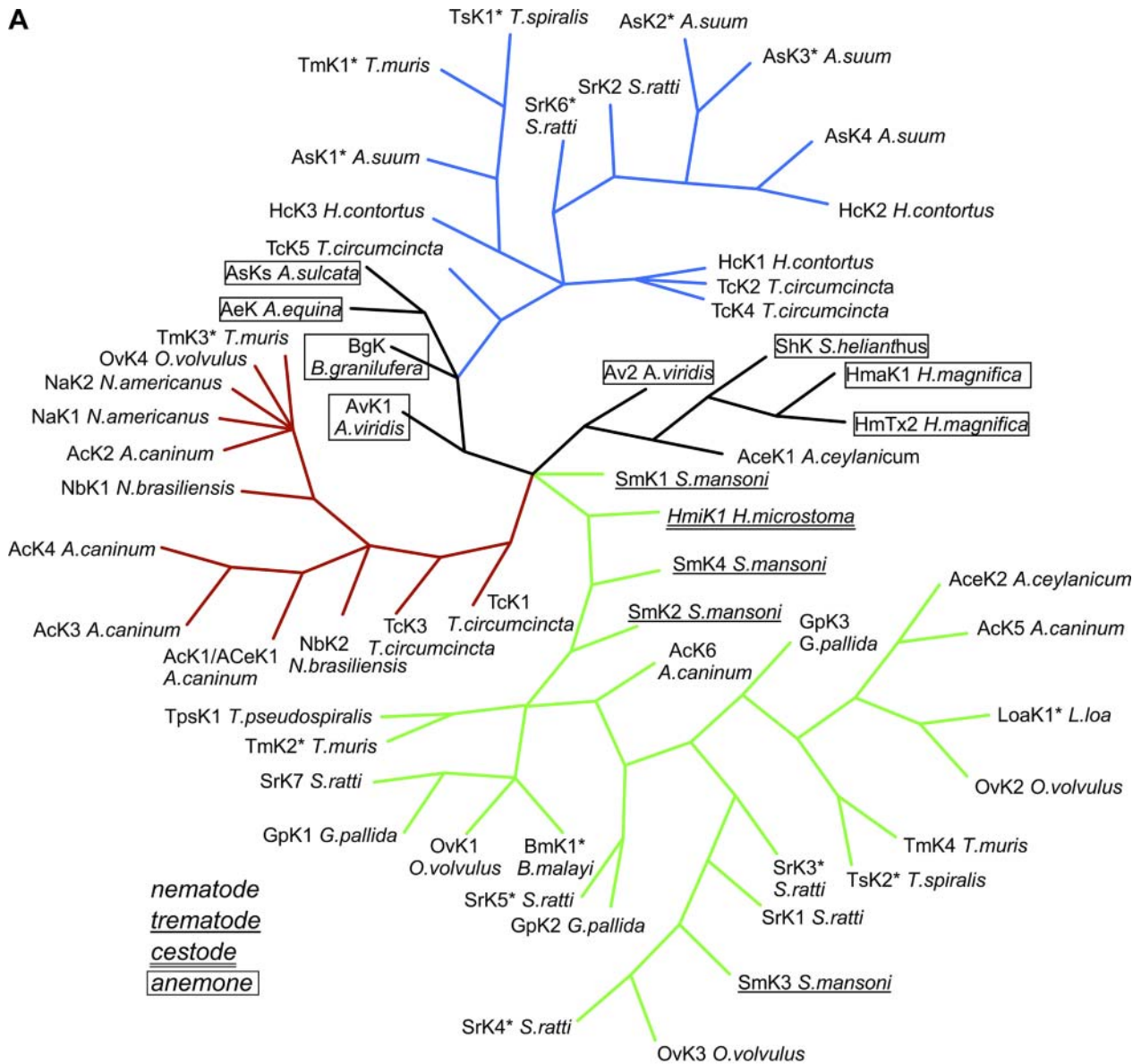
Since Kv1.3 blockers have immunomodulatory effects similar to those ascribed to worm infections (1), we investigated whether worm ShKTs share structural similarity to ShK, block Kv1.3, and exhibit immunomodulatory activity. In this report, we describe a large family of parasitic worm ShKTs. We determined the structure of 2 of these ShKTs and demonstrated that they block Kv1.3 channels, selectively suppress the function of T_{EM} cells *in vitro*, and inhibit DTH. It is therefore plausible that ShK-like worm peptides are among the active agents that contribute to the protective effect of parasitic worms in autoimmune diseases.

MATERIALS AND METHODS

Identification of ShK-like worm sequences and phylogenetic analysis

To identify secreted hookworm proteins that might be injected into the host and mediate host–parasite interactions, we dissected the anterior secretory glands of the parasitic hookworm *Ancylostoma caninum* and created a full-length SMART cDNA library. Two thousand clones chosen randomly were sequenced by using Sanger-based cycle sequencing, and a customized bioinformatic pipeline was used to clean, cluster, and annotate the sequences. The most abundant transcript encoding a secreted protein with at least 1 ShK-like domain, *Ancylostoma caninum* K1 (AcK1), was used to search in genome databases, which resulted in our identifying 53 related protein sequences from diverse parasitic worms that infect humans, cattle, dogs, goats, sheep, and rodents. Supplemental Fig. S1 shows a manually produced alignment of these protein sequences. Most are secreted peptides, whereas others (indicated by asterisks) represent domains within larger worm proteins. We subjected this alignment to parsimony analysis with the Phylogenetic Analysis Using Parsimony (PAUP*) 4.0b101 program (55). One thousand replicates of heuristic searches with random sequence addition yielded a family of the shortest trees of 386 sequences in length, and the tree shown in **Fig. 1A** is the majority-rule consensus tree of this group.

Figure 1. ShK-like protein sequences in parasitic worms. *A)* Phylogenetic tree of peptides and protein domains from nematodes, trematodes, and cestodes and their relationship to sea anemone toxins. This is a majority-rule consensus tree from the family of shortest trees found by extensive parsimony searching using the computer program PAUP*, v4.0b10 (55). Sequences that represent domains within larger proteins are indicated by asterisks. *B)* Aligned sequences of AcK1, ACeK1, BmK1, BmK2, and AcKt1, together with BgK, ShK, and MMP23$_{Tx}$. Note that the peptide sequence of AcK1 from dog-infecting *A. caninum* is identical with that of ACeK1 from human-infecting *A. ceylanicum*. BmK2 and AcK1t are analogues of BmK1 and AcK1, which we designed and synthesized. BMK2 was generated based on the structures of AcK1 and BmK1, and our knowledge of the ShK channel interaction surface; it differs from BmK1 at just 5 residues and is C-terminally amidated. AcK1t is a truncated version of AcK1 that lacks the first 9 residues. The alignments were produced manually and cover only the region spanning the 6 cysteines contained within this domain. The conserved cysteines are highlighted in gray, the critical pore-protruding K/R residue is highlighted in magenta and the neighboring aromatic residue present in many Kv channel-blocking peptides is highlighted in green. Other conserved residues are highlighted in yellow.

Peptide synthesis, folding, and purification

Peptides were synthesized on a Prelude synthesizer (Protein Technologies, Tucson, AZ, USA). Each peptide was assembled on Rink-mBHA resin (Peptides International, Louisville, KY, USA), by using Fmoc-tBu chemistry with 6-Cl-HOBT diisopropyl carbodiimide activation of each amino acid derivative. Following removal of the final Fmoc protecting group, the peptides were cleaved and simultaneously deprotected with reagent K for 2 h. The peptide was isolated from the spent resin by filtration over a Buchner funnel. The crude product was precipitated in ice-cold diethyl ether, dissolved in 50% acetic acid (AcOH) in H_2O, and diluted in water containing 5% methyl alcohol and 1 mM glutathione (a mixture of reduced and oxidized). In the case of AcK1, solubilization required neat trifluoroacetic acid (TFA) to fully dissolve the product. Solubilization in 50% AcOH resulted in a viscous hydrogel. The pH was adjusted to 8.0 with NH_4OH, and the peptides were allowed to fold oxidatively for 48 h. Each product was subsequently purified by preparative reverse-phase–high-performance liquid chromatography (RP-HPLC). Fractions containing each peptide were assayed by analytical RP-HPLC (Supplemental Fig. S2), and those with purity >95% were combined and lyophilized. Peptide identity was confirmed by ESI-MS and was consistent with theory for formation of 3 disulfide bonds for each peptide.

Expression and purification of AcK1

The synthesized oligonucleotide sequence of mature AcK1 was purchased from GeneArt (Life Technologies, Carlsbad, CA, USA) and subsequently cloned into pET-32a plasmid (EMD4Biosciences-Novagen, Billerica, MA, USA). The transformed BL21 (DE3) cells were grown at 37°C until the OD_{600} reached 0.6. Isopropyl β-D-1-thiogalactopyranoside (IPTG) was added to a final optimized concentration of 1 mM, and expression was carried out at 28°C for 6 h. For isotopic labeling, the cells were grown in minimal medium containing $^{15}NH_4Cl$ and ^{13}C-glucose (Cambridge Isotope Labs, Andover, MA, USA) and expressed at 20°C for 12 h. The cultures were centrifuged at 5000 g at 4°C for 10 min, and the supernatant was discarded. The cell pellets were stored at −80°C until purification.

For a 1 L culture, a cell pellet was resuspended and lysed in BugBuster (EMD4Biosciences-Novagen) (5 ml/g of cell pellet) at room temperature for 1 h, with the addition of EDTA-free protease inhibitor cocktail (Roche Diagnostics, Indianapolis, IN, USA). The lysate was centrifuged at 20,000 g for 20 min at 4°C. The supernatant was loaded onto a nickel Sepharose column (GE Healthcare Bio-Sciences, Pittsburgh, PA, USA) and washed with buffer [20 mM Na_2HPO_4 (pH 8.0), 0.5 M NaCl, and 20 mM imidazole] for removal of any nonspecific binding. The fusion protein was then eluted with elution buffer [20 mM Na_2HPO_4 (pH 8.0), 0.5 M NaCl, and 250 mM imidazole]. The fraction containing fusion protein was dialyzed extensively in dialysis buffer [50 mM Tris (pH 8.0), 50 mM NaCl, and 1 mM EDTA] over 24 h. Final yields of fusion protein from 1 L varied from 60 to 80 mg. Tobacco etch virus (150 μg TEV) protease was added to cleave the fusion protein at room temperature for 20 h. The cleaved protein was then loaded onto a C18 RP-HPLC column (100×10 mm; Phenomenex, Lane Cove, NSW, Australia) equilibrated in 95% buffer A (99.9% water and 0.01% TFA) and 5% buffer B (20% water, 80% acetonitrile, and 0.01% TFA). AcK1 was eluted with an acetonitrile gradient (35–45% over 10 min). Eluted fractions containing AcK1 were lyophilized for storage. Peptide concentrations were determined using the bicinchoninic acid (BCA) assay (Pierce, Rockford, IL, USA) with bovine serum albumin as a standard. The BCA assay was calibrated against peptide content by amino acid analysis (The Florey Institute of Neuroscience and Mental Health, Parkville, VIC, Australia). Peptide purity and mass were determined by analytical RP-HPLC and LC-MS, respectively.

Nuclear magnetic resonance (NMR) spectroscopy

AcK1

Samples of 1 mM $^{15}N,^{13}C$-labeled AcK1 were prepared in 10 mM Na_2HPO_4 in either 100% $^{2}H_2O$ or 90%/10% $H_2O/^{2}H_2O$ at pH 5.4. Experiments were performed at 25°C on Avance 500, 600, and 800 spectrometers (Bruker Corp., Billerica, MA, USA), each equipped with a cryoprobe and z-axis gradient. AcK1 gave good-quality spectra at pH 5.4 and 25°C, 1-dimensional (1D) ^{1}H and 2-dimensional (2D) ^{1}H-^{15}N HSQC spectra are shown in Supplemental Fig. S3A, B, E. Backbone and side-chain assignments were obtained with the following triple-resonance experiments: HNCO, HNCA, HNCACB, HN(CO)CA, and CBCA(CO)NH. Side chain assignments were made using the HBHA(CBCACO)NH experiment in combination with 3-dimensional (3D) ^{15}N-resolved, 3D ^{13}C(aliphatic)-resolved, and 3D ^{13}C(aromatic)-resolved [$^{1}H,^{1}H$]-nuclear Overhauser effect spectroscopy (NOESY) experiments recorded at 800 MHz, with a mixing time of 150 ms. A 2D-NOESY spectrum was also recorded at 600 MHz, with a mixing time of 150 ms and used in addition to the 3D NOESY experiments for final structure calculations. NMR spectra were processed using TOPSPIN (version 3.2; Bruker) and analyzed with XEASY (available at https://sbgrid.org/software/title/XEASY). Spectra were referenced to dioxane at 3.75 ppm.

Brugia malayi K1 (BmK1)

Lyophilized samples of synthetic BmK1 were dissolved in either 100% $^{2}H_2O$ or 90%/10% $H_2O/^{2}H_2O$ buffered with 10 mM Na_2HPO_4 (pH 4.8), to a final concentration of ∼0.8 mM. Similar to AcK1, good-quality spectra were obtained for BmK1; 1D and ^{1}H-^{15}N HSQC spectra are shown in Supplemental Fig. S3C, D, F. Chemical shift assignments for backbone and side-chain proton resonances were made by conventional sequential assignment procedures from analysis of the 2D [^{1}H-^{1}H]-total-correlation spectroscopy (TOCSY; spin lock time, 30 and 70 ms) and [^{1}H-^{1}H]-NOESY spectra (mixing time, 200 ms) acquired at 20°C. ^{15}N chemical shifts were obtained from a ^{1}H-^{15}N-HSQC spectrum, and ^{13}C chemical shifts were obtained from a combination of ^{13}C-H2BC and ^{13}C-HSQC spectra acquired in 100% $^{2}H_2O$ (pH 4.8). A 2D-NOESY spectrum was also recorded at 800 MHz with a mixing time of 200 ms at pH 5.8 and was subsequently used for final structure calculations. For determination of the amide resonance temperature coefficients, a series of 1D ^{1}H spectra and 2D homonuclear TOCSY spectra (spin lock time, 70 ms) was acquired at 15, 20, 25, and 30°C on an Avance 600 MHz instrument (Bruker). Amide exchange rates were monitored by dissolving freeze-dried material in $^{2}H_2O$ at pH 4.8 and then recording a series of 1D spectra, followed by a 70 ms TOCSY spectrum at 20°C. All spectra were processed in TOPSPIN (version 3.2) and were analyzed by CcpNmr-Analysis (version 2.1.5; available at http://www.ccpn.ac.uk/software/analysis/). The NMR chemical shift data reported in this article have been deposited in the BioMagResBank Data Bank (56) with accession numbers 19460 and 19450 for AcK1 and BmK1, respectively.

Structure calculations

Structures were initially calculated by using the noeassign macro within the program CYANA 3.0 (57). Disulfide bond constraints were added according to the connectivity patterns observed from the structures calculated in the absence of disulfide constraints; NOEs were also observed directly between cysteine protons across all 3 disulfide bonds in AcK1 and BmK1; for both AcK1 and BmK1, the pattern of disulfide connectivity was 1–6/2–4/3–5, as observed for ShK (58). Torsion angle constraints (φ and φ) were generated from an analysis of chemical shifts by using Talos+/TALOS-N (59). Structures were then calculated with Xplor-NIH 2.33 (60), using a simulated annealing protocol in torsion angle dynamics (TAD). A radius of gyration term to represent weak packing potential was included, as were database potentials of mean force to refine against multidimensional torsion angles (61), Cα and Cβ chemical shifts, and backbone hydrogen-bonding. One hundred trial structures were calculated initially from a minimized extended structure, with random initial velocities and a starting temperature of 50,000 K. A further 100 refined structures were subsequently calculated, starting from the lowest energy folded structure of the previous calculation and refined using TAD, starting from an initial temperature of 3000 K. Additional backbone distance constraints were explicitly included for BmK1 if a hydrogen bond to the same acceptor was observed in more than 50% of the structures calculated with the inclusion of the hydrogen bond database potential in automatic detection mode and if the amide displayed slow solvent exchange or a low temperature coefficient. Structures were selected on the basis of lowest NOE and dihedral angle violations and ranked according to total energy. The accepted structures had no NOE violations >0.15 Å (AcK1) or 0.3 Å (BmK1) or dihedral angle violations >4° (BmK1) or >3° (AcK1). Thirty structures were selected based on the total lowest energy and assessed using MOLMOL (version 2K.1) (62) and ProcheckNMR (63). Structural statistics are summarized in Supplemental Table S1. Molecular representations were prepared using either Chimera (64) or PyMOL (The PyMOL Molecular Graphics System, Version 1.5.0.4 Schrödinger, LLC, Portland, OR, USA; available at http://www.pymol.org).

Coordinates for the final sets of 30 structures for AcK1 and BmK1, as well as the NMR restraints from which the structures were calculated, have been deposited in the Protein Data Bank (65) with the ID codes 2MD0 and 2MCR, respectively (http://www.rcsb.org/).

Analysis of the pharmacological block of Kvs by parasitic worm peptides

Pharmacological analysis was performed for Kv1.1, -1.2, -1.3, -1.6, and -3.2, expressed in mammalian cells by using whole-cell, patch-clamp recordings (EPC-9; HEKA Elektronik, Lambrecht, Germany). Each of the channel clones and cell lines used for these studies has been characterized and described previously (2, 17). Kv1.3 currents were recorded from both human T cells and from L929 fibroblast cells stably expressing cloned mouse Kv1.3 channels. Mouse Kv1.1 channels were stably expressed in L929 and rat Kv1.2 channels in B82 fibroblasts cells. Human Kv1.6 and rat Kv3.2 channels were transiently transfected into L929 cells along with eGFP1 (to visualize transfection success), by using TransIT-LT1 transfection reagent (Mirus Bio, Madison, WI, USA), whereas the human K2P3.1 (a gift from Dr. Diana Bautista, University of California, Berkeley, CA, USA), Nav1.5, and KCa3.1 channels were transfected into COS-7 cells. All currents were recorded using the whole-cell recording configuration in normal mammalian Ringer solution containing 140 mM Na$^+$. For all Kv channel recordings, the pipette solution contained (in mM): 145 KF, 10 HEPES, 10 EGTA, and 2 MgCl$_2$ (pH 7.2) in 300 mOsM and currents were elicited by 200 ms depolarizing pulses from a holding potential of −80 to +40 mV, as described previously (2). The Nav1.5 and K2P3.1 channels were recorded with CsF and KCl internal solutions, respectively, and the KCa3.1 channels were recorded with K-aspartate internal solution with 1 μM free Ca^{2+}. Nav1.5 currents were elicited by a test pulse to 0 mV from a −80 mV holding potential every 1 s. K2P3.1 and KCa3.1 currents were elicited by a 200 ms voltage ramp from −120 to +80 mV every 10 s. Each channel blocker was tested at multiple concentrations prepared in serial dilutions from peptide stocks dissolved in P6N buffer [10 mM NaHPO$_4$, 0.8% NaCl, and 0.05% Tween-20 (pH 6.0)] (19). The measured reduction in peak current at 40 mV for each concentration was normalized to that of the control normal mammalian Ringer solution and used to generate a dose–response curve. The IC$_{50}$ values were determined with SigmaPlot (Systat Software, Inc., Chicago, IL, USA) by fitting the dose–response curve with the user-defined equation $f = [1 + (x/\mathrm{IC}_{50})^n]^{-1}$, where f is the fractional current at x concentration of peptides, and n is the Hill coefficient. Pipette resistances averaged 2 MΩ, and series resistance compensation of 80% was used at all current levels. Acquisition and analysis were performed with IGOR Pro (WaveMetrics, Lake Oswego, OR, USA) and Excel (Microsoft, Redmond, WA, USA). Data are presented as means ± SE.

Cells

The Lewis rat ovalbumin-specific T$_{EM}$ lymphocyte cell line transduced with GFP (66) was a gift from Dr. Alexander Flügel (Georg-August University, Göttingen, Germany). This cell line up-regulates Kv1.3 on activation with ovalbumin and causes DTH *in vivo*, and ShK-186 suppresses its proliferation and *in vivo* activation and migration during a DTH response (12). Histopaque-1077 gradients (Sigma-Aldrich, St. Louis, MO, USA) were used to isolate splenocytes from 5- to 7-wk-old female Lewis rats. These predominantly CCR7$^+$ T cells are resistant to ShK-186 because they up-regulate the KCa3.1 channel on activation. All experiments involving rats were approved by the institutional animal care and use committee at Baylor College of Medicine.

[^{3}H] thymidine incorporation assays

T-lymphocyte proliferation was measured by incorporation of [^{3}H] thymidine in the DNA of dividing cells (2). The Lewis rat ovalbumin-specific T$_{EM}$ lymphocyte cell line transduced with GFP (12, 67) was maintained in culture by alternating cycles of antigen-induced stimulation and cytokine-dependent expansion. The T$_{EM}$ cells were used after 4 d of cytokine-dependent expansion. Splenic T cells were used immediately after collection. The cells were seeded in flat-bottomed, 96-well plates in 200 μl of culture medium supplemented with 1% homologous rat serum. ShK or BmK2 was added to the cells 30 min before the antigen or mitogen. The T$_{EM}$ cells were stimulated with 10 μg/ml ovalbumin in the presence of irradiated thymocytes as antigen-presenting cells, and splenocytes were stimulated with 1 μg/ml concanavalin A. The cells were cultured for 3 d and were pulsed with [^{3}H] thymidine (1 μCi/well) 16–18 h before harvest on glass fiber filters. The proliferative response of T cells was assessed in a β-scintillation counter.

DTH

Female Lewis rats were purchased from Charles River Laboratories (Wilmington, MA, USA) and housed under clean

conditions in autoclaved setups with food and water *ad libitum*. Active DTH was induced in 8- to 9-wk-old Lewis rats by immunization in the flank with an emulsion of ovalbumin with complete Freund's adjuvant (2, 3, 17, 19). Seven days later, while under isoflurane anesthesia, the animals were challenged with ovalbumin dissolved in saline in one ear and saline in the other. The rats received a single dose of vehicle or BmK2 (0.5 mg/kg dissolved in vehicle) in the scruff of the neck at the time of the challenge. Ear thickness was determined 24 h later with a spring-loaded micrometer as a measure of inflammation.

Cytokine production by human T cells

We compared the effects of the worm peptides with ShK-186 in an assay used previously to assess the effect of ShK-186 on human T cells (19). When human T cells are activated, the $CCR7^+$ T cells in the pool up-regulate KCa3.1 channels during activation and escape inhibition by Kv1.3 blockers (1–4, 19). Protein kinase C signaling is responsible for KCa3.1 up-regulation (68). Thapsigargin, a SERCA pump inhibitor, triggers calcium signaling and increases cytokine production without activating the protein kinase C pathway necessary for KCa3.1 up-regulation (4, 19). We had shown that ShK-186 is very effective in suppressing cytokine production (IL2 = IFN-γ>IL17>IL4) in this assay (4, 19). We therefore stimulated human T cells with thapsigargin to assess the effect of the worm peptides on the production of a representative cytokine (IFN-γ) in unseparated human T cells from 3 separate donors. ShK-186, BmK2, and truncated AcK1 (AcK1t) solutions were reconstituted in P6N (19) and diluted in complete DMEM (25 mM HEPES, 2 mM L-glutamine, 55 μM β-mercaptoethanol, and 100 IU penicillin and streptomycin) at 4 times the desired final concentration. Fifty microliters of each dilution was added to 4 replicate wells of a 96-well tissue culture plate, and 50 μl of medium was added to replicate negative and positive control wells. To initiate the experiment, we added 100 μl of whole blood to each. The samples were incubated overnight with the drug at 37°C, 5% CO_2, after which the cells were stimulated. We added 50 μl of the ×4 thapsigargin stimulus (40 μM) to all wells, except to the negative control wells, to which 50 μl of 0.4% DMSO was added (19). The plate was incubated for 48 h at 37°C and 5% CO_2 and spun down for 5 min at 1500 rpm, and the supernatant was transferred to a fresh 96-well plate. ELISA was used to measure cytokine concentrations with the following monoclonal antibodies from Biolegend (San Diego, CA, USA): anti-human IFN-γ NIB42 and NS.B3 for capture and detection.

RESULTS

Screening cDNA libraries and genome databases

We screened a cDNA library of anterior secretory glands of the parasitic hookworm *A. caninum*, a close relative of the human hookworms *A. duodenale*, *A. ceylanicum*, and *Necator americanus*. We sequenced more than 2000 randomly selected clones, which were clustered into 159 unique transcripts. Nine transcripts encoded secreted proteins with a single ShK/*Bunodosoma granulifera* toxin (BgK)-like domain and predicted masses of 6.9-8.3 kDa. Of these, AcK1 (Fig. 1*B*) was the most abundant transcript, with 27 ESTs, ranking 13th among the transcripts coding for putative secreted

proteins in the library. We used AcK1 to search within genome databases and discovered several related sequences in many parasitic worms that infect humans and other mammals. Supplemental Fig. S1 shows an alignment of 53 ShK-like worm sequences, and 8 known channel-blocking, ShK-related peptides from sea anemones. Most of these are independent peptides, whereas others represent domains within larger proteins (indicated by asterisks). The alignment (Supplemental Fig. 1) shows strong conservation of an Asp (Asp5 in ShK) in the majority of the worm peptides and sea anemones. In ShK, the carboxylate of this Asp is close to the ε-ammonium group of Lys30, and this interaction facilitates proper folding of the peptide (58, 69). A positively charged residue and an adjacent aromatic/hydrophobic residue [Lys22/Tyr23 in ShK and Arg/Leu in toxin domain of matrix metalloprotease 23 ($MMP23_{TxD}$)] are necessary for potent Kv1.3 channel blockade (16, 18, 20). Of the 53 worm sequences, only 17 have this dyad; AcK1 contains Lys/Leu and BmK1 contains Lys/Tyr at the equivalent positions (Supplemental Fig. S1). Peptides lacking these critical residues may block other ion channels in preference to Kv1.3, although peptides lacking the dyad have been reported to block K^+ channels (70). AcK1 from the dog-infecting hookworm *A. caninum* and ACeK1 from the human-infecting hookworm *A. ceylanicum* (Supplemental Fig. S1) have identical protein sequences (96% DNA sequence identity), and this common sequence will henceforth be referred to as AcK1.

The parsimony-based phylogenetic tree in Fig. 1*A* shows the inferred evolutionary relatedness of these 60 sequences. The anemone sequences form 2 separate branches (shown in black) that join the tree at a point close to its center, and the various worm species form 3 separate branches, distinguished in red, green, and blue, which emanate near this point. No systematic differences were found in the distribution on this tree of peptides *vs.* domains. The trematode and cestode sequences are on a single branch (green), whereas nematode sequences are represented on all 3 branches (Fig. 1*A*). Note that different peptides from a single species of worm may be distributed on very distant branches of this tree, notably those from *Strongyloides ratti*, *Trichuris muris*, *Onchocerca volvulus*, and *A. caninum*. This observation suggests that the oldest gene duplications that have diversified this family of peptides predate the divergence of the worm species.

Synthesis of AcK1, BmK1, and analogues

We selected 2 worm peptides for further study from 2 branches of the phylogenetic tree (Fig. 1 and Supplemental Fig. S1). AcK1 was selected because it is a peptide (like ShK), rather than a domain in a larger protein, and is expressed in the anterior secretory glands of both the dog- and human-infecting hookworms *A. caninum* and *A. ceylanicum*, respectively, suggesting that it is injected into the host

during infection by the worm; also, *A. caninum* ameliorates disease in a mouse model of colitis (34). BmK1, from a filarial worm, was selected because it represents an ShKT domain in a zinc metalloprotease like MMP23 (MMP23$_{TxD}$) (20), and filarial worms are reported to modulate the human immune response in infected patients (71). AcK1 and BmK1 were synthesized by solid-phase peptide synthesis, and AcK1 was expressed recombinantly to allow isotopic labeling for NMR studies (Figs. S2*A*). Neither synthetic nor recombinant AcK1 folded smoothly; the crude product required more stringent conditions to solubilize, and the folding profile was much more complex than that of ShK or BmK1. A truncated AcK1 analogue lacking the first 9 N-terminal residues (AcK1t; Supplemental Fig. S2*B*) was easier to fold and yielded a well-resolved, hydrophilic-eluting product. BmK1 folded much like ShK-related peptides, into a more hydrophilic product with misfolded species eluting at later times (Supplemental Fig. S2*C*). BmK2, an analogue of BmK1 that we designed based on sequence alignment and our knowledge of the ShK-channel interaction surface (4, 16–18, 58), differs from BmK1 by 5 residues (Fig. 1*B*) and is folded, with a major peak eluting in the middle of the folding profile (22 min; Supplemental Fig. S2*D*).

Solution structures of AcK1 and BmK1

Supplemental Table S1 summarizes the experimental constraints and structural statistics for AcK1 and BmK1. Both structures are well defined and are of good quality, as judged by low deviations from idealized geometry and Lennard-Jones potentials, indicating that the structures have favorable nonbonded contacts. Furthermore, 92 and 89%, respectively, of the residues in AcK1 and BmK1 lie in the most favored regions of the Ramachandran plots. The first 10 residues of AcK1 are defined by 114 NOE constraints and form an extended structure (RMS over the backbone heavy atoms N, Cα, and C′, ~1.2 Å). However, the absence of long-range NOEs and the paucity of medium-range ones (only 7 observed), combined with strong sequential H$^\alpha$-H^N and H^N-H^N NOEs, indicate that this region undergoes conformational exchange and is not well defined relative to the structured core of the molecule. Based on chemical shifts, Talos-N predicts that residues 2–7 are dynamic, and this was further confirmed by the backbone ^{15}N[^{1}H] NOE data (Supplemental Fig. S3*G*).

Figure 2*A* shows the families of structures for AcK1 and BmK1, and Fig. 2*B* highlights the locations of charged side chains on their respective molecular surfaces. **Figure 3***A* compares the closest-to-average struc-
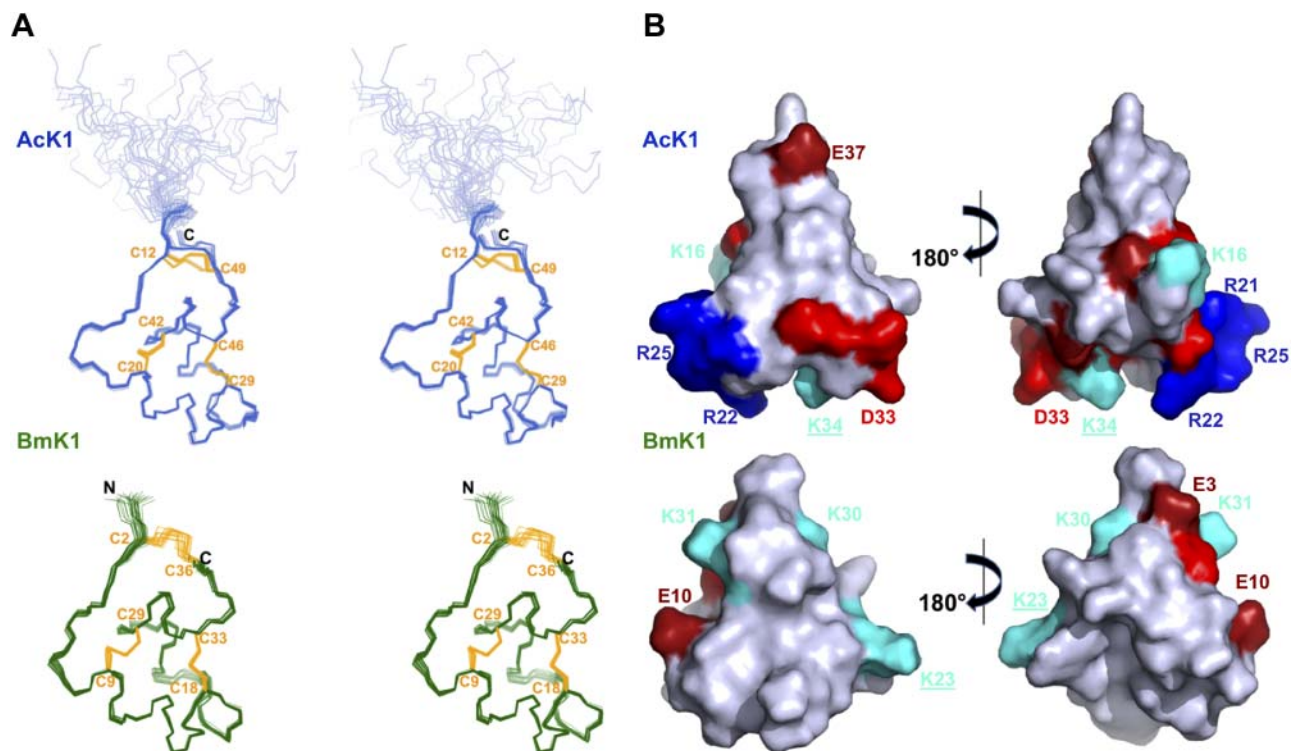

Figure 2. Solution structures of AcK1 and BmK1. *A*) Stereo views of the families of 30 final structures; top panels show AcK1 in blue, bottom panels show BmK1 in green. Structures are superimposed over backbone heavy atoms of residues 11–51 of AcK1 and 2–36 of BmK1. Disulfide bonds are gold. For AcK1 2, helices were defined (residues 20–25 and 32–41) by both MOLMOL (62) and SSTRUC (http://tardis.nibio.go.jp/joy/sstruc.html); MOLMOL also identified 2 short 3$_{10}$ helix-encompassing residues 3–6 and 28–30 in AcK1. For BmK1, 3 helices were defined for residues 9–13, 17–20, and 22–28 by both programs. *B*) Surface representation of AcK1 (top) and BmK1 (bottom) generated using PyMOL (http://www.pymol.org). Surfaces show basic residues in blue (Arg in dark blue and Lys in light blue) and acidic residues in red. The 2 views are related by a 180° rotation about the vertical axis. The putative critical lysine in each peptide is underlined.
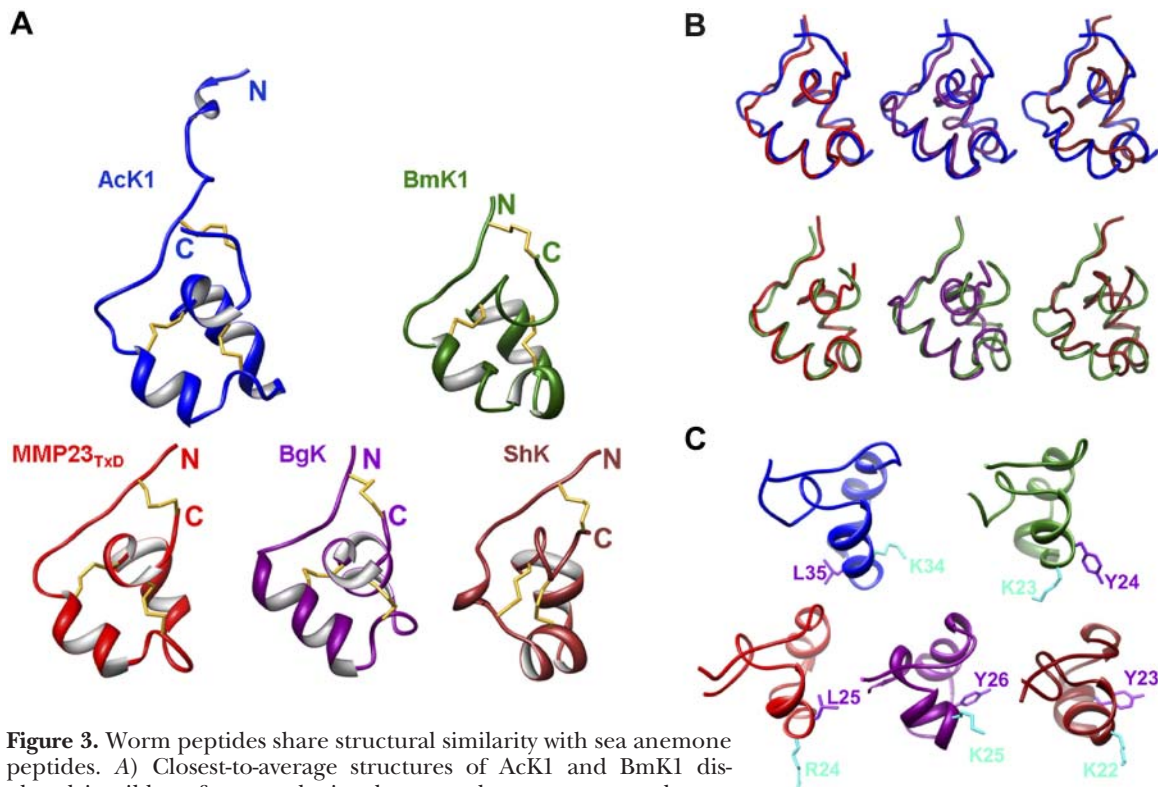
Figure 3. Worm peptides share structural similarity with sea anemone peptides. *A*) Closest-to-average structures of AcK1 and BmK1 displayed in ribbon form to depict the secondary structure and compared with that of BgK (Protein Data Bank ID 1BGK), MMP23$_{TxD}$ (2K72), and ShK (1ROO). N and C = N and C termini, respectively. RMS deviations for AcK1 and BmK1 *vs.* MMP23$_{TxD}$, BgK, and ShK are shown in Supplemental Table S2. *B*) Comparison of the backbones of the closest-to-average structures of AcK1 (blue) and BmK1 (green) with those of MMP23$_{TxD}$, BgK, and ShK. Structures are superimposed over backbone heavy atoms of residues 12–49 of AcK1, 2–36 of BmK1, 2–37 of MMP23, and 2–35 of ShK by using Chimera (64). The superimpositions of closest-to-average structures are as follows: AcK1 (blue) with MMP23$_{TxD}$ (red; top left), BgK1 (magenta; top middle), and ShK (dark red; top right). BmK1 (green) with MMP23$_{TxD}$ (red; bottom left), BgK1 (magenta; bottom middle), and ShK (dark red; bottom right). AcK1 and BmK1 share greater structural similarity with MMP23$_{TxD}$ (RMS deviations over the backbone heavy atoms N, Cα, C′ are 2.38 and 1.39 Å, respectively) than with BgK or ShK, as documented in Supplemental Table S2. *C*) Closest-to-average structures of AcK1 (blue), BmK1 (green), MMP23$_{TxD}$ (red), BgK (magenta), and ShK (dark red). Structures were aligned with reference to the BmK1 structure using structure-based sequence alignment in Chimera (64). The locations of the 2 side chains in each peptide that correspond to the Lys22/Tyr23 dyad that is important for Kv1 blockade in ShK are shown.

tures of AcK1 and BmK1 with those of BgK (72, 73), ShK (58), and MMP23$_{TxD}$ (20). These peptides have low sequence similarity (~19%) but share the same disulfide framework and critical pore-blocking, positively charged Lys/Arg residue. Furthermore, all structures are predominantly helical, although the lengths and exact positions of the helical elements differ slightly among the 5 structures. The structures are compared in more detail in Fig. 3*B* and the differences are quantified in Supplemental Table S2. Some differences in secondary structure between the worm peptides and ShK are apparent (Fig. 3*B*); in particular, a four-residue insert in both of the worm peptides (as well as BgK and MMP23$_{TxD}$) is absent in ShK, which produces a shorter interhelical loop 2 in this peptide. The close structural similarity of BmK1 and MMP23$_{TxD}$ may reflect the fact that both are extracellular domains of metalloproteases (20). The critical lysine and other key residues in ShK that are essential for K$^+$ channel blockade (4, 17, 18) are located on a short helical region, but the side chains of residues in the Lys22/Tyr23 dyad

(73), which is important for Kv1 blockade in ShK, have different relative orientations in the parasitic worm peptides and MMP23$_{TxD}$ compared with BgK and ShK (Fig. 3*C*). These differences may contribute to the lower potency of the worm peptides (**Fig. 4*A*, *B***) and MMP23$_{TxD}$, compared with that of ShK, BgK, and their analogues.

As noted above, Asp5 is almost completely conserved in the sequences shown in Supplemental Fig. S1, although in a few sequences it is conservatively replaced with Asn, Glu, or Ser. The residue equivalent to Lys30 in ShK is largely conserved among the sequences (Supplemental Fig. S1), although Val occupies this position in AcK1, which may contribute to the less efficient oxidative folding of this peptide *in vitro* compared with ShK and BmK1 (which contains Lys at this position). The pKa of Asp5 in ShK-[K30A] is approximately half a unit higher than in native ShK (69), supporting an Asp5-Lys30 electrostatic interaction in ShK; this may exist in BmK1 but cannot be present in AcK1. Replacement of Val34 with Lys in AcK1 promoted the formation of an Asp-Lys interaction, leading
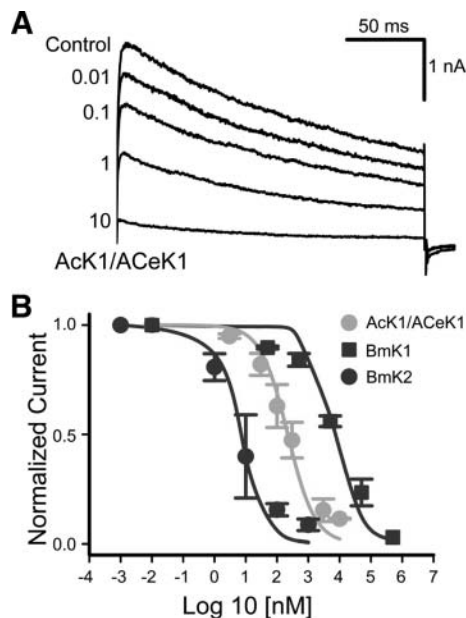
Figure 4. Kv1.3 potassium channel inhibition. *A*) AcK1 blocks Kv1.3 channels in human T cells. *B*) Dose–response curves for blocking Kv1.3 in human T cells by AcK1, BmK1, and BmK2. Data are presented as means ± SEM.

to a >10-fold improvement in the yield of the desired folded peptide (data not shown). The N-terminal extension in AcK1 is less ordered than the disulfide-bridged core and is poorly defined relative to the core structure, at least in solution. It also appears to be unnecessary for K$^+$-channel blocking activity, because its elimination in AcK1t does not affect Kv1.3 blocking-potency (**Table 1**).

Electrophysiological analysis of AcK1, BmK1, and analogues

AcK1, its truncated analogue AcK1t, BmK1, and BmK2 blocked cloned Kv1.3 channels expressed heterologously in mammalian cells and also native Kv1.3 channels in human T cells, in a dose-dependent manner with a Hill coefficient of 1 (Fig. 4*A*, *B*). AcK1, AcK1t,

and BmK2 blocked Kv1.3 with IC$_{50}$ values in the low- to midnanomolar range, while BmK1 blocked the channel at low micromolar concentrations (Fig. 4*B*). The block was partially reversible. Compared to BgK, the worm peptides exhibited equal (BmK2) to 1000-fold (BmK1) lower potency against Kv1.3 (Table 1). Compared to ShK-186, the worm peptides exhibited 20- (BmK2) to 80,000-fold lower potency against Kv1.3 (Table 1). BmK2, the most potent Kv1.3 blocker among these peptides, exhibited >4000-fold selectivity for Kv1.3 over the closely related Kv1.1, Kv1.2, and Kv1.6 channels, as well as over the more distantly related Kv3.2, KCa3.1 (KCNN4), and K2P3.1 (KCNK3, TASK1) channels and the cardiac sodium channel Na$_V$1.5 (Table 1). This selectivity profile was similar to ShK-186 (Table 1).

Immunomodulatory activity of parasitic worm peptides

Kv1.3 blockers suppress the proliferation of Kv1.3-expressing CCR7$^-$ T$_{EM}$ cells without affecting CCR7$^+$ naive and central memory T cells, because these latter cells up-regulate the KCa3.1 channel during activation (1, 3, 6, 68). Since AcK1t and BmK2 block Kv1.3 and not KCa3.1 (Fig. 4), these 2 peptides should have similar effects. We assessed the immunomodulatory effect of AcK1t and BmK2 with the same assays that were used to evaluate ShK-186 (4, 12, 19). AcK1t, BmK2, and ShK-186 suppressed ovalbumin-stimulated [^{3}H] thymidine proliferation of an ovalbumin-specific rat CCR7$^-$ T$_{EM}$ cell line that up-regulates Kv1.3 on activation (12). Suppression was achieved at concentrations of ShK-186 (10 nM), AcK1t (1 μM), and BmK2 (1 μM) that blocked >90% of Kv1.3 channels (Figs. 4*B* and 5*A*). AcK1t, BmK2, and ShK-186 did not suppress concanavalin-A-stimulated [^{3}H] thymidine incorporation in CCR7$^+$ T cells that up-regulate KCa3.1 channels on activation (Fig. 5*B*) (2, 6, 68).

ShK-186 exhibits *in vivo* immunomodulatory activity in numerous rodent models (1–3, 8–15) including DTH. We selected DTH as the assay to assess the immunomodulatory activity of worm ShKTs. We previously used live 2-photon imaging to demonstrate that

TABLE 1. IC$_{50}$ *values of AcK1, BmK1, BmK2, BgK, ShK, ShK-186, margatoxin, and aurelin on a panel of ion channels*

Channel (IUPHAR/HUGO)	Peptide (nM)							
	ShK	ShK-186	BgK	Margatoxin	BmK1	BmK2	AcK1/ACeK1[a]	Aurelin
Kv1.1/KCNA1	0.028	7	6	10	ND	1500	>1500	ND
Kv1.2/KCNA2	10	48	15	0.520	ND	>5000[b]	ND	ND
Kv1.3/KCNA3	0.01	0.069	10	0.110	6900	3.6	266	4120
Kv1.6/KCNA6	0.2	18	ND	>100	ND	3700	ND	ND
Kv3.2/KCNC2	5	20	ND	>100	ND	>4000[c]	ND	ND
KCa3.1/KCNN4	20	>100	172	>100	ND	>2000	ND	ND
K2P3.1/KCNK3	ND	>100	ND	ND	ND	>2000	ND	ND
Nav1.5/SCN5A	ND	>100	ND	ND	ND	>2000	ND	ND

Hill coefficient was 1 in all cases. Margatoxin is a scorpion toxin that blocks both Kv1.3 and Kv1.2 with picomolar affinity. Aurelin, a ShKT peptide from jellyfish, shares phylogenetic and structural similarity to ShK, BgK (76), and worm ShKTs. Each peptide was assessed on ≥3 independent cells, and ≥3 dose points were obtained for each cell to determine the IC$_{50}$ value for each worm ShKt. ND, not determined. [a]AcKt1 blocked Kv1.3 with an IC$_{50}$ value of 395 nM. [b]BmK2 at 5 μM produced 0% block. [c]BmK2 at 4 μM produced <5% block.
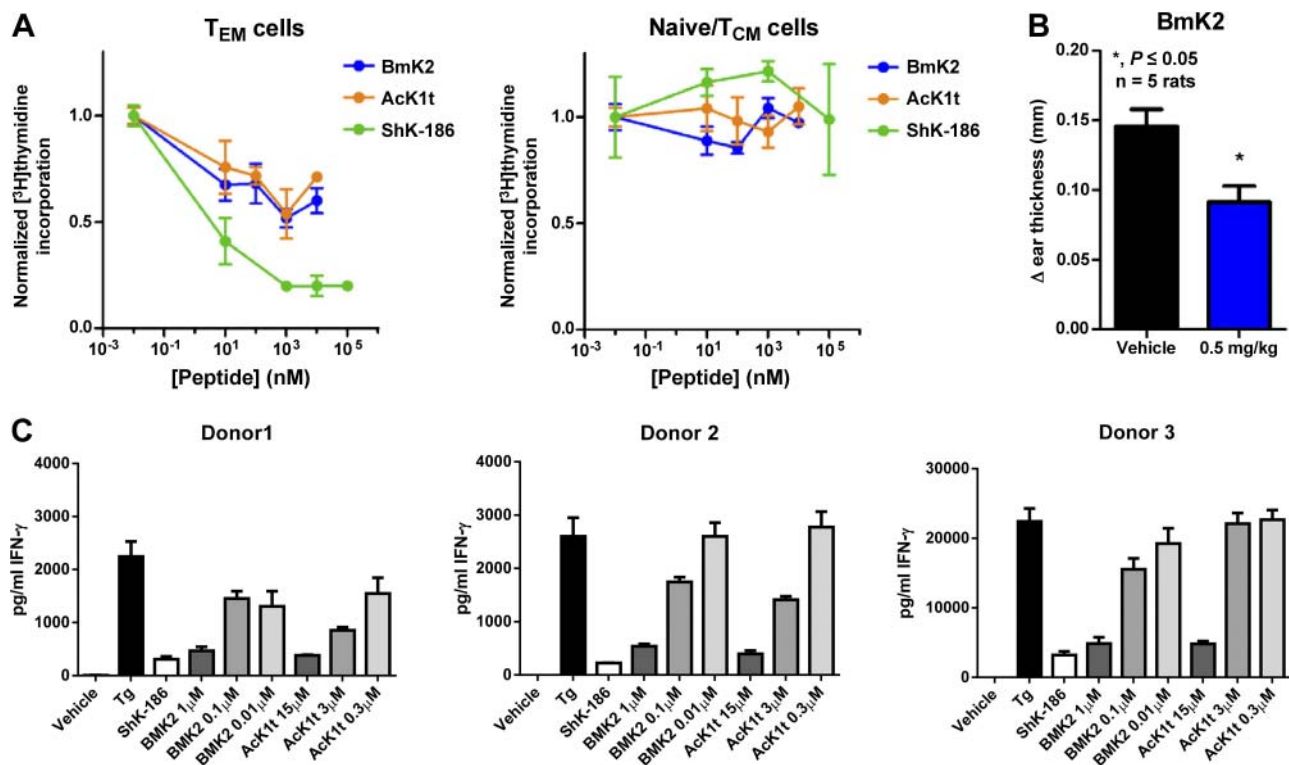
Figure 5. Preferential suppression of human T_{EM} cells and cytokine production. *A*) Effect of AcK1t and BmK2 on proliferation of concanavalin A-activated rat splenocytes (predominantly $CCR7^+$ naive$+T_{CM}$ cells) *vs.* ovalbumin-activated $CCR7^-$ ovalbumin-specific rat T_{EM} cells. Proliferation assays were performed in triplicate in 3 independent experiments. *B*) Effect of BmK2 on active DTH in rats ($n = 6$). Six rats per group were used. *C*) Effect of AcK1t and BmK2 on IFN-γ production by thapsigargin-stimulated human T cells from 3 separate donors. Data are expressed as means ± SEM.

ShK-186 suppressed DTH by blocking Kv1.3 channels in skin-homing T_{EM} cells (12). BmK2 is phylogenetically related to ShK-186, has a structure remarkably similar to that of ShK, is the most potent worm ShKT blocker of Kv1.3, and preferentially suppresses T_{EM} cells, and we therefore assessed its ability to inhibit DTH (12). Administration of BmK2 at the time of antigen challenge suppressed active DTH in rats, as shown in Fig. 5*B*.

We also evaluated the effect of the worm peptides on human T cells using assays identical to those used to evaluate ShK-186 (4, 19). When entire human T cells are used (*i.e.*, without separation into $CCR7^-$ and $CCR7^+$ T cells), the $CCR7^+$ T cells in the pool up-regulate KCa3.1 channels during activation and escape inhibition by Kv1.3 blockers (1, 3, 4, 19). However, if thapsigargin, a SERCA pump inhibitor is used to stimulate human T cells, calcium signaling is triggered and cytokine production augmented without up-regulating the KCa3.1 channel (4, 19). We previously used this assay to screen the effect of ShK-186 on human T cells and therefore used it to assess the worm ShKTs (4, 19). AcK1t, BmK2, and ShK-186 suppressed thapsigargin-stimulated IFN-γ production by human T cells from 3 healthy donors in a dose-dependent manner (Fig. 5*C*). In summary, worm peptides preferentially suppress T_{EM} cell responses both *in vitro* and *in vivo* in rats and humans.

DISCUSSION

ShK, a peptide from the sea anemone *S. helianthus*, blocks Kv1.3 K^+ channels in T cells and preferentially suppresses the function of T_{EM} cells, both *in vitro* and *in vivo*. ShK-186, a synthetic analogue of ShK, is effective in multiple rodent models of autoimmune diseases and has been successfully tested in human phase 1 trials in healthy volunteers (1–4, 6, 8–15). In this report, we describe an extensive family of ShKTs (ShK-related peptides and domains) in all 3 groups of worms that infect humans: nematodes, trematodes, and cestodes. We provide the first structural characterization of representatives of this family: a secreted peptide that is present in both human-infecting (*A. ceylanicum*) and dog-infecting (*A. caninum*) hookworms (AcK1) and a domain from a metalloprotease from the filarial worm *B. malayi* (BmK1). These ShKTs adopt predominantly helical structures resembling ShK, with closest structural similarity to $MMP23_{TxD}$, the ShKT of the mammalian metalloprotease MMP23. They block Kv1.3 channels with nanomolar-to-micromolar potency and a high degree of specificity. Like other Kv1.3 blockers, they preferentially inhibit the proliferation of T_{EM} cells, suppress cytokine production, and inhibit DTH.

A significant concern with worm therapy is that any beneficial effects have to be balanced against the potentially harmful changes that result from worm infec-

tions (21, 22, 32, 52). For example, probiotic worm therapy with the hookworm *N. americanus* causes diarrhea, vomiting, and intestinal pain when more than 50 larvae are administered (44). This problem of administering pathogenic parasitic worms could be circumvented by the identification and characterization of immunomodulatory worm molecules and by the development of these or related molecules as therapeutics for autoimmune diseases. Although several worm extracts are active in rodent models of autoimmune diseases (26, 31, 34, 38, 40, 43, 45, 46, 48, 51), only 4 worm-derived immunomodulatory molecules have been characterized. Of these, macrophage inhibitory factor worsens autoimmune diseases, cytostatins suppress T_H2 responses and would presumably not be effective in most autoimmune diseases (31, 43), neutrophil inhibitory factor (26, 45, 46) has not been evaluated in autoimmune disease models, and ES-62 is the only worm molecule to date that has been shown to be effective in animal models of autoimmune diseases (38).

Four lines of evidence suggest that Kv1.3-blocking worm ShKTs also contribute to the beneficial effects of probiotic worm therapy. First, disease-associated T cells in patients with MS, type-1 diabetes, RA, psoriasis, and chronic asthma are activated T_{EM} cells with an elevated number of functional Kv1.3 channels (1, 3, 6) and can be modulated by Kv1.3-blocking worm ShKTs. Second, Kv1.3 channels play a critical role in regulating proliferation, proinflammatory cytokine production, cytotoxic function, and *in vivo* migration of both $CD4^+$ and $CD8^+$ T_{EM} cells (1–4, 6, 8, 12, 17, 19). Worm ShKTs such as ShK-186 suppress proliferation of T_{EM} cells without affecting KCa3-1–up-regulating $CCR7^+$ T cell subsets and decrease proinflammatory T_H1 cytokines (2, 4, 6, 12, 17, 19, 68). Third, worm ShKTs such as ShK-186 suppress DTH, mostly likely *via* their preferential suppressive action on T_{EM} cells (1, 3, 12). These effects are unlikely to be due to effects on macrophages or B cells, as macrophages express a Kv1.3/Kv1.5 heteromultimer (74) that is likely to be significantly less sensitive to Kv1.3-selective blockers, and naive and early memory B cells are insensitive to Kv1.3 blockers because they up-regulate KCa3.1 channels when they are activated (1, 75). Kv1.3-selective blockers also ameliorate disease in rodent models of DTH, MS, RA, type-1 diabetes mellitus, contact dermatitis, autoimmune glomerulonephritis, psoriasis, chronic asthma, and inflammatory bone resorption due to periodontitis (2, 3, 9, 11, 12, 17, 19). In addition, Kv1.3 knockout mice are resistant to the development of MS-like disease. Finally, genetic deletion or dominant-negative suppression of Kv1.3 results in differentiation into IL-10-secreting regulatory T cells *via* up-regulation of SMAD3 phosphorylation (10). This effect is similar to the induction of regulatory T cells during probiotic worm therapy (35, 48).

In summary, we have characterized a novel class of immunomodulators present in all 3 groups of parasitic worms that infect humans. We have defined their evolutionary relationships, determined structures of representative peptides, defined their molecular target (Kv1.3), and demonstrated their selective suppressive function on T_{EM} cells that are implicated in autoimmune diseases. These worm peptides or related peptides, such as ShK-186 (4, 17), could supersede probiotic worm-based therapies by retaining the beneficial effects and eliminating the harmful effects associated with parasitic infections. [Fj]

REFERENCES

1. Cahalan, M. D., and Chandy, K. G. (2009) The functional network of ion channels in T lymphocytes. *Immunol. Rev.* **231,** 59–87
2. Beeton, C., Pennington, M. W., Wulff, H., Singh, S., Nugent, D., Crossley, G., Khaytin, I., Calabresi, P. A., Chen, C. Y., Gutman, G. A., and Chandy, K. G. (2005) Targeting effector memory T cells with a selective peptide inhibitor of Kv1.3 channels for therapy of autoimmune diseases. *Mol. Pharmacol.* **67,** 1369–1381
3. Beeton, C., Wulff, H., Standifer, N. E., Azam, P., Mullen, K. M., Pennington, M. W., Kolski-Andreaco, A., Wei, E., Grino, A., Counts, D. R., Wang, P. H., LeeHealey, C. J., Andrews, B. S., Sankaranarayanan, A., Homerick, D., Roeck, W. W., Tehranzadeh, J., Stanhope, K. L., Zimin, P., Havel, P. J., Griffey, S., Knaus, H. G., Nepom, G. T., Gutman, G. A., Calabresi, P. A., and Chandy, K. G. (2006) Kv1.3 channels are a therapeutic target for T cell-mediated autoimmune diseases. *Proc. Natl. Acad. Sci. U.S.A.* **103,** 17414–17419
4. Chi, V., Pennington, M. W., Norton, R. S., Tarcha, E. J., Londono, L. M., Sims-Fahey, B., Upadhyay, S. K., Lakey, J. T., Iadonato, S., Wulff, H., Beeton, C., and Chandy, K. G. (2012) Development of a sea anemone toxin as an immunomodulator for therapy of autoimmune diseases. *Toxicon* **59,** 529–546
5. Hu, L., Pennington, M., Jiang, Q., Whartenby, K. A., and Calabresi, P. A. (2007) Characterization of the functional properties of the voltage-gated potassium channel Kv1.3 in human $CD4^+$ T lymphocytes. *J. Immunol.* **179,** 4563–4570
6. Wulff, H., Calabresi, P. A., Allie, R., Yun, S., Pennington, M., Beeton, C., and Chandy, K. G. (2003) The voltage-gated Kv1.3 K^+ channel in effector memory T cells as new target for MS. *J. Clin. Invest.* **111,** 1703–1713
7. Rus, H., Pardo, C. A., Hu, L., Darrah, E., Cudrici, C., Niculescu, T., Niculescu, F., Mullen, K. M., Allie, R., Guo, L., Wulff, H., Beeton, C., Judge, S. I., Kerr, D. A., Knaus, H. G., Chandy, K. G., and Calabresi, P. A. (2005) The voltage-gated potassium channel Kv1.3 is highly expressed on inflammatory infiltrates in multiple sclerosis brain. *Proc. Natl. Acad. Sci. U.S.A.* **102,** 11094–11099
8. Azam, P., Sankaranarayanan, A., Homerick, D., Griffey, S., and Wulff, H. (2007) Targeting effector memory T cells with the small molecule Kv1.3 blocker PAP-1 suppresses allergic contact dermatitis. *J. Invest. Dermatol.* **127,** 1419–1429
9. Beeton, C., Wulff, H., Barbaria, J., Clot-Faybesse, O., Pennington, M., Bernard, D., Cahalan, M. D., Chandy, K. G., and Beraud, E. (2001) Selective blockade of T lymphocyte K^+ channels ameliorates experimental autoimmune encephalomyelitis, a model for multiple sclerosis. *Proc. Natl. Acad. Sci. U.S.A.* **98,** 13942–13947

10. Gocke, A. R., Lebson, L. A., Grishkan, I. V., Hu, L., Nguyen, H. M., Whartenby, K. A., Chandy, K. G., and Calabresi, P. A. (2012) Kv1.3 deletion biases T cells toward an immunoregulatory phenotype and renders mice resistant to autoimmune encephalomyelitis. *J. Immunol.* **188,** 5877–5886

11. Koshy, S., Huq, R., Tanner, M. R., Atik, M. A., Porter, P. C., Khan, F. S., Pennington, M. W., Hanania, N. A., Corry, D. B., and Beeton, C. (2014) Blocking Kv1.3 channels inhibits Th2 lymphocyte function and treats a rat model of asthma. *J. Biol. Chem.* **289,** 12623–12632

12. Matheu, M. P., Beeton, C., Garcia, A., Chi, V., Rangaraju, S., Safrina, O., Monaghan, K., Uemura, M. I., Li, D., Pal, S., de la Maza, L. M., Monuki, E., Flugel, A., Pennington, M. W., Parker, I., Chandy, K. G., and Cahalan, M. D. (2008) Imaging of effector memory T cells during a delayed-type hypersensitivity reaction and suppression by Kv1.3 channel block. *Immunity* **29,** 602–614

13. Ren, Y. R., Pan, F., Parvez, S., Fleig, A., Chong, C. R., Xu, J., Dang, Y., Zhang, J., Jiang, H., Penner, R., and Liu, J. O. (2008) Clofazimine inhibits human Kv1.3 potassium channel by perturbing calcium oscillation in T lymphocytes. *PloS One* **3,** e4009

14. Upadhyay, S. K., Eckel-Mahan, K. L., Mirbolooki, M. R., Tjong, I., Griffey, S. M., Schmunk, G., Koehne, A., Halbout, B., Iadonato, S., Pedersen, B., Borrelli, E., Wang, P. H., Mukherjee, J., Sassone-Corsi, P., and Chandy, K. G. (2013) Selective Kv1.3 channel blocker as therapeutic for obesity and insulin resistance. *Proc. Natl. Acad. Sci. U.S.A.* **110,** E2239–E2248

15. Valverde, P., Kawai, T., and Taubman, M. A. (2004) Selective blockade of voltage-gated potassium channels reduces inflammatory bone resorption in experimental periodontal disease. *J. Bone Miner. Res.* **19,** 155–164

16. Kalman, K., Pennington, M. W., Lanigan, M. D., Nguyen, A., Rauer, H., Mahnir, V., Paschetto, K., Kem, W. R., Grissmer, S., Gutman, G. A., Christian, E. P., Cahalan, M. D., Norton, R. S., and Chandy, K. G. (1998) ShK-Dap22, a potent Kv1.3-specific immunosuppressive polypeptide. *J. Biol. Chem.* **273,** 32697–32707

17. Pennington, M. W., Beeton, C., Galea, C. A., Smith, B. J., Chi, V., Monaghan, K. P., Garcia, A., Rangaraju, S., Giuffrida, A., Plank, D., Crossley, G., Nugent, D., Khaytin, I., Lefievre, Y., Peshenko, I., Dixon, C., Chauhan, S., Orzel, A., Inoue, T., Hu, X., Moore, R. V., Norton, R. S., and Chandy, K. G. (2009) Engineering a stable and selective peptide blocker of the Kv1.3 channel in T lymphocytes. *Mol. Pharmacol.* **75,** 762–773

18. Rauer, H., Pennington, M., Cahalan, M., and Chandy, K. G. (1999) Structural conservation of the pores of calcium-activated and voltage-gated potassium channels determined by a sea anemone toxin. *J. Biol. Chem.* **274,** 21885–21892

19. Tarcha, E. J., Chi, V., Munoz-Elias, E. J., Bailey, D., Londono, L. M., Upadhyay, S. K., Norton, K., Banks, A., Tjong, I., Nguyen, H., Hu, X., Ruppert, G. W., Boley, S. E., Slauter, R., Sams, J., Knapp, B., Kentala, D., Hansen, Z., Pennington, M. W., Beeton, C., Chandy, K. G., and Iadonato, S. P. (2012) Durable pharmacological responses from the peptide ShK-186, a specific Kv1.3 channel inhibitor that suppresses T cell mediators of autoimmune disease. *J. Pharmacol. Exp. Ther.* **342,** 642–653

20. Rangaraju, S., Khoo, K. K., Feng, Z. P., Crossley, G., Nugent, D., Khaytin, I., Chi, V., Pham, C., Calabresi, P., Pennington, M. W., Norton, R. S., and Chandy, K. G. (2010) Potassium channel modulation by a toxin domain in matrix metalloprotease 23. *J. Biol. Chem.* **285,** 9124–9136

21. Weinstock, J. V. (2012) Autoimmunity: the worm returns. *Nature* **491,** 183–185

22. Harnett, W., and Harnett, M. M. (2010) Helminth-derived immunomodulators: can understanding the worm produce the pill? *Nat. Rev. Immunol.* **10,** 278–284

23. World Health Organization (2014) Soil-transmitted helminthiases: number of children treated in 2012.. *Wkly. Epidemiol. Rec.* **89,** 133–140

24. Summers, R. W., Elliott, D. E., Urban, J. F., Jr., Thompson, R., and Weinstock, J. V. (2005) *Trichuris suis* therapy in Crohn's disease. *Gut* **54,** 87–90

25. Summers, R. W., Elliott, D. E., Urban, J. F., Jr., Thompson, R. A., and Weinstock, J. V. (2005) *Trichuris suis* therapy for active ulcerative colitis: a randomized controlled trial. *Gastroenterology* **128,** 825–832

26. Anbu, K. A., and Joshi, P. (2008) Identification of a 55 kDa *Haemonchus contortus* excretory/secretory glycoprotein as a neutrophil inhibitory factor. *Parasite Immunol.* **30,** 23–30

27. Boitelle, A., Scales, H. E., Di Lorenzo, C., Devaney, E., Kennedy, M. W., Garside, P., and Lawrence, C. E. (2003) Investigating the impact of helminth products on immune responsiveness using a TCR transgenic adoptive transfer system. *J. Immunol.* **171,** 447–454

28. Broadhurst, M. J., Leung, J. M., Kashyap, V., McCune, J. M., Mahadevan, U., McKerrow, J. H., and Loke, P. (2010) IL-22$^+$ CD4$^+$ T cells are associated with therapeutic *Trichuris trichiura* infection in an ulcerative colitis patient. *Sci. Transl. Med.* **2,** 60ra88

29. Chu, K. M., Watermeyer, G., Shelly, L., Janssen, J., May, T. D., Brink, K., Benefeld, G., and Li, X. (2013) Childhood helminth exposure is protective against inflammatory bowel disease: a case control study in South Africa. *Inflamm. Bowel Dis.* **19,** 614–620

30. Correale, J., and Farez, M. (2007) Association between parasite infection and immune responses in multiple sclerosis. *Ann. Neurol.* **61,** 97–108

31. Cox, G. M., Kithcart, A. P., Pitt, D., Guan, Z., Alexander, J., Williams, J. L., Shawler, T., Dagia, N. M., Popovich, P. G., Satoskar, A. R., and Whitacre, C. C. (2013) Macrophage migration inhibitory factor potentiates autoimmune-mediated neuroinflammation. *J. Immunol.* **191,** 1043–1054

32. Dunne, D. W., and Cooke, A. (2005) A worm's eye view of the immune system: consequences for evolution of human autoimmune disease. *Nat. Rev. Immunol.* **5,** 420–426

33. Elliott, D. E., and Weinstock, J. V. (2012) Where are we on worms? *Curr. Opin. Gastroenterol.* **28,** 551–556

34. Ferreira, I., Smyth, D., Gaze, S., Aziz, A., Giacomin, P., Ruyssers, N., Artis, D., Laha, T., Navarro, S., Loukas, A., and McSorley, H. J. (2013) Hookworm excretory/secretory products induce interleukin-4 (IL-4)$^+$ IL-10$^+$ CD4$^+$ T cell responses and suppress pathology in a mouse model of colitis. *Infect. Immun.* **81,** 2104–2111

35. Fleming, J. O., Isaak, A., Lee, J. E., Luzzio, C. C., Carrithers, M. D., Cook, T. D., Field, A. S., Boland, J., and Fabry, Z. (2011) Probiotic helminth administration in relapsing-remitting multiple sclerosis: a phase 1 study. *Mult. Scler.* **17,** 743–754

36. Gaze, S., McSorley, H. J., Daveson, J., Jones, D., Bethony, J. M., Oliveira, L. M., Speare, R., McCarthy, J. S., Engwerda, C. R., Croese, J., and Loukas, A. (2012) Characterising the mucosal and systemic immune responses to experimental human hookworm infection. *PLoS Pathog.* **8,** e1002520

37. Goodridge, H. S., Wilson, E. H., Harnett, W., Campbell, C. C., Harnett, M. M., and Liew, F. Y. (2001) Modulation of macrophage cytokine production by ES-62, a secreted product of the filarial nematode *Acanthocheilonema viteae. J. Immunol.* **167,** 940–945

38. Harnett, M. M., Melendez, A. J., and Harnett, W. (2010) The therapeutic potential of the filarial nematode-derived immunomodulator, ES-62 in inflammatory disease. *Clin. Exp. Immunol.* **159,** 256–267

39. Hartmann, S., Kyewski, B., Sonnenburg, B., and Lucius, R. (1997) A filarial cysteine protease inhibitor down-regulates T cell proliferation and enhances interleukin-10 production. *Eur. J. Immunol.* **27,** 2253–2260

40. Hernandez, J. L., Leung, G., and McKay, D. M. (2013) Cestode regulation of inflammation and inflammatory diseases. *Int. J. Parasitol.* **43,** 233–243

41. Johnston, M. J., Wang, A., Catarino, M. E., Ball, L., Phan, V. C., MacDonald, J. A., and McKay, D. M. (2010) Extracts of the rat tapeworm, *Hymenolepis diminuta* suppress macrophage activation in vitro and alleviate chemically induced colitis in mice. *Infect. Immun.* **78,** 1364–1375

42. La Flamme, A. C., Ruddenklau, K., and Backstrom, B. T. (2003) Schistosomiasis decreases central nervous system inflammation and alters the progression of experimental autoimmune encephalomyelitis. *Infect. Immun.* **71,** 4996–5004

43. Llamas-Covarrubias, M. A., Valle, Y., Bucala, R., Navarro-Hernandez, R. E., Palafox-Sanchez, C. A., Padilla-Gutierrez, J. R., Parra-Rojas, I., Bernard-Medina, A. G., Reyes-Castillo, Z., and Munoz-Valle, J. F. (2013) Macrophage migration inhibitory factor (MIF): genetic evidence for participation in early onset and early stage rheumatoid arthritis. *Cytokine* **61,** 759–765

44. Mortimer, K., Brown, A., Feary, J., Jagger, C., Lewis, S., Antoniak, M., Pritchard, D., and Britton, J. (2006) Dose-ranging study for trials of therapeutic infection with *Necator americanus* in humans. *Am. J. Trop. Med. Hyg.* **75,** 914–920

45. Moyle, M., Foster, D. L., McGrath, D. E., Brown, S. M., Laroche, Y., De Meutter, J., Stanssens, P., Bogowitz, C. A., Fried, V. A., Ely, J. A., and et al. (1994) A hookworm glycoprotein that inhibits neutrophil function is a ligand of the integrin CD11b/CD18. *J. Biol. Chem.* **269,** 10008–10015

46. Muchowski, P. J., Zhang, L., Chang, E. R., Soule, H. R., Plow, E. F., and Moyle, M. (1994) Functional interaction between the integrin antagonist neutrophil inhibitory factor and the I domain of CD11b/CD18. *J. Biol. Chem.* **269,** 26419–26423

47. Rosche, B., Wernecke, K. D., Ohlraun, S., Dorr, J. M., and Paul, F. (2013) *Trichuris suis* ova in relapsing-remitting multiple sclerosis and clinically isolated syndrome (TRIOMS): study protocol for a randomized controlled trial. *Trials* **14,** 112

48. Ruyssers, N. E., De Winter, B. Y., De Man, J. G., Loukas, A., Pearson, M. S., Weinstock, J. V., Van den Bossche, R. M., Martinet, W., Pelckmans, P. A., and Moreels, T. G. (2009) Therapeutic potential of helminth soluble proteins in TNBS-induced colitis in mice. *Inflamm. Bowel Dis.* **15,** 491–500

49. Sandborn, W. J., Elliott, D. E., Weinstock, J., Summers, R. W., Landry-Wheeler, A., Silver, N., Harnett, M. D., and Hanauer, S. B. (2013) Randomised clinical trial: the safety and tolerability of *Trichuris suis* ova in patients with Crohn's disease. *Aliment. Pharmacol. Ther.* **38,** 255–263

50. Sewell, D., Qing, Z., Reinke, E., Elliot, D., Weinstock, J., Sandor, M., and Fabry, Z. (2003) Immunomodulation of experimental autoimmune encephalomyelitis by helminth ova immunization. *Int. Immunol.* **15,** 59–69

51. Teixeira-Carvalho, A., Fujiwara, R. T., Stemmy, E. J., Olive, D., Damsker, J. M., Loukas, A., Correa-Oliveira, R., Constant, S. L., and Bethony, J. M. (2008) Binding of excreted and/or secreted products of adult hookworms to human NK cells in *Necator americanus*-infected individuals from Brazil. *Infect. Immun.* **76,** 5810–5816

52. Zaccone, P., and Cooke, A. (2013) Vaccine against autoimmune disease: can helminths or their products provide a therapy? *Curr. Opin. Immunol.* **25,** 418–423

53. Wu, S., Li, R. W., Li, W., Beshah, E., Dawson, H. D., and Urban, J. F., Jr. (2012) Worm burden-dependent disruption of the porcine colon microbiota by *Trichuris suis* infection. *PloS One* **7,** e35470

54. Leung, J. M., and Loke, P. (2013) A role for IL-22 in the relationship between intestinal helminths, gut microbiota and mucosal immunity. *Int. J. Parasitol.* **43,** 253–257

55. Swofford, D. L. (2003) PAUP*: Phylogenetic Analysis Using Parsimony (and Other Methods), ver. 4 Beta. Sinauer Associates, Sunderland, MA, USA

56. Ulrich, E. L., Akutsu, H., Doreleijers, J. F., Harano, Y., Ioannidis, Y. E., Lin, J., Livny, M., Mading, S., Maziuk, D., Miller, Z., Nakatani, E., Schulte, C. F., Tolmie, D. E., Kent Wenger, R., Yao, H., and Markley, J. L. (2008) BioMagResBank. *Nucleic Acids Res.* **36,** D402–D408

57. Guntert, P. (2004) Automated NMR structure calculation with CYANA. *Methods Mol. Biol.* **278,** 353–378

58. Tudor, J. E., Pallaghy, P. K., Pennington, M. W., and Norton, R. S. (1996) Solution structure of ShK toxin, a novel potassium channel inhibitor from a sea anemone. *Nat. Struct. Biol.* **3,** 317–320

59. Shen, Y., and Bax, A. (2013) Protein backbone and sidechain torsion angles predicted from NMR chemical shifts using artificial neural networks. *J. Biomol. NMR.* **56,** 227–241

60. Schwieters, C. D., Kuszewski, J. J., Tjandra, N., and Clore, G. M. (2003) The Xplor-NIH NMR molecular structure determination package. *J. Magn. Reson.* **160,** 65–73

61. Kuszewski, J., Gronenborn, A. M., and Clore, G. M. (1996) Improving the quality of NMR and crystallographic protein structures by means of a conformational database potential derived from structure databases. *Protein Sci.* **5,** 1067–1080

62. Koradi, R., Billeter, M., and Wüthrich, K. (1996) MOLMOL: a program for display and analysis of macromolecular structures. *J. Mol. Graph.* **14,** 29–32, 51–55

63. Laskowski, R. A., Rullmannn, J. A., MacArthur, M. W., Kaptein, R., and Thornton, J. M. (1996) AQUA and PROCHECK-NMR: programs for checking the quality of protein structures solved by NMR. *J. Biomol. NMR.* **8,** 477–486

64. Pettersen, E. F., Goddard, T. D., Huang, C. C., Couch, G. S., Greenblatt, D. M., Meng, E. C., and Ferrin, T. E. (2004) UCSF Chimera–a visualization system for exploratory research and analysis. *J. Comput. Chem.* **25,** 1605–1612

65. Berman, H. M., Westbrook, J., Feng, Z., Gilliland, G., Bhat, T. N., Weissig, H., Shindyalov, I. N., and Bourne, P. E. (2000) The Protein Data Bank. *Nucleic Acids Res.* **28,** 235–242

66. Kawakami, N., Odoardi, F., Ziemssen, T., Bradl, M., Ritter, T., Neuhaus, O., Lassmann, H., Wekerle, H., and Flugel, A. (2005) Autoimmune $CD4^+$ T cell memory: lifelong persistence of encephalitogenic T cell clones in healthy immune repertoires. *J. Immunol.* **175,** 69–81

67. Flugel, A., Willem, M., Berkowicz, T., and Wekerle, H. (1999) Gene transfer into $CD4^+$ T lymphocytes: green fluorescent protein-engineered, encephalitogenic T cells illuminate brain autoimmune responses. *Nat. Med.* **5,** 843–847

68. Ghanshani, S., Wulff, H., Miller, M. J., Rohm, H., Neben, A., Gutman, G. A., Cahalan, M. D., and Chandy, K. G. (2000) Up-regulation of the IKCa1 potassium channel during T-cell activation: molecular mechanism and functional consequences. *J. Biol. Chem.* **275,** 37137–37149

69. Tudor, J. E., Pennington, M. W., and Norton, R. S. (1998) Ionisation behaviour and solution properties of the potassium-channel blocker ShK toxin. *Eur. J. Biochem.* **251,** 133–141

70. Huys, I., Olamendi-Portugal, T., Garcia-Gomez, B. I., Vandenberghe, I., Van Beeumen, J., Dyason, K., Clynen, E., Zhu, S., van der Walt, J., Possani, L. D., and Tytgat, J. (2004) A subfamily of acidic α-K^+ toxins. *J. Biol. Chem.* **279,** 2781–2789

71. Wammes, L. J., Hamid, F., Wiria, A. E., Wibowo, H., Sartono, E., Maizels, R. M., Smits, H. H., Supali, T., and Yazdanbakhsh, M. (2012) Regulatory T cells in human lymphatic filariasis: stronger functional activity in microfilaremics. *PLoS Negl. Trop. Dis.* **6,** e1655

72. Cotton, J., Crest, M., Bouet, F., Alessandri, N., Gola, M., Forest, E., Karlsson, E., Castaneda, O., Harvey, A. L., Vita, C., and Menez, A. (1997) A potassium-channel toxin from the sea anemone *Bunodosoma granulifera*, an inhibitor for Kv1 channels. Revision of the amino acid sequence, disulfide-bridge assignment, chemical synthesis, and biological activity. *Eur. J. Biochem.* **244,** 192–202

73. Dauplais, M., Lecoq, A., Song, J., Cotton, J., Jamin, N., Gilquin, B., Roumestand, C., Vita, C., de Medeiros, C. L., Rowan, E. G., Harvey, A. L., and Menez, A. (1997) On the convergent evolution of animal toxins. Conservation of a diad of functional residues in potassium channel-blocking toxins with unrelated structures. *J. Biol. Chem.* **272,** 4302–4309

74. Vicente, R., Villalonga, N., Calvo, M., Escalada, A., Solsona, C., Soler, C., Tamkun, M. M., and Felipe, A. (2008) Kv1.5 association modifies Kv1.3 traffic and membrane localization. *J. Biol. Chem.* **283,** 8756–8764

75. Wulff, H., Knaus, H. G., Pennington, M., and Chandy, K. G. (2004) K^+ channel expression during B cell differentiation: implications for immunomodulation and autoimmunity. *J. Immunol.* **173,** 776–786

76. Ovchinnikova, T. V., Balandin, S. V., Aleshina, G. M., Tagaev, A. A., Leonova, Y. F., Krasnodembsky, E. D., Men'shenin, A. V., and Kokryakov, V. N. (2006) Aurelin, a novel antimicrobial peptide from jellyfish *Aurelia aurita* with structural features of defensins and channel-blocking toxins. *Biochem. Biophys. Res. Commun.* **348,** 514–523